Solid Particle Erosion of an Fe-Fe_3C Metal Matrix Composite

B.A. LINDSLEY and A.R. MARDER

The erosion resistance and morphology of spheroidized Fe-C alloys containing 0.2 to 1.4 wt pct carbon was investigated. The Fe-C alloy system was chosen as a model metal-matrix composite for the study of the effect on erosion of a hard second phase in a ductile matrix. Alloys were austenitized and water quenched to form martensite, then tempered at 690 °C for different times to produce carbide sizes of 0.4, 0.8, 1.6, and 2.4 μm. Utilizing these materials, it was found that the erosion resistance increased as the microstructural features decreased in size, with the important microstructural variables being carbide spacing and ferrite grain size. These variables control dislocation motion in the ferrite and, in turn, affect the plastic deformation and the erosion resistance of the spheroidized alloys. For the 0.4 to 1.4 pct C alloys, the carbide spacing was sufficient to determine erosion rate, whereas, for the 0.2 pct C alloys, ferrite grain size became the controlling structure. Microstructural spacing, which is a measure of the mean free path between both the grain boundaries and the carbides, was found to describe all of the erosion data. A Hall–Petch-type relationship was found between microstructural spacing and both erosion rate and hardness.

I. INTRODUCTION

THE definition of erosion by the American Society for Testing and Materials is the ''progressive loss of original material from a solid surface due to the mechanical interaction between that surface and a fluid, a multicomponent fluid, or *impinging* liquid or *solid particles*.''[1] At low impingement angles, material is removed by a cutting or platelet mechanism.[2,3,4] Erosion of ductile materials at high or normal impact angles requires substantial work hardening of the surface layer before any material is removed,[5–8] and it has been found that the erosion rate is dependent on the depth of deformation and the increase in surface hardness.[8] A mix of two mechanisms is believed to occur in the erosion of ductile materials, with the cutting/platelet mechanism dominating at low angles, the work hardening mechanism dominating at high angles, and a combination of the two at intermediate angles.

The material effects on erosion resistance, with respect to both mechanical and morphological variables, remain unclear. Finnie *et al.*[9] found a direct correlation between the erosion resistance of pure metals and their hardness. Additional evidence supports this finding, where the eroded surface hardness is related to the erosion rate.[10] However, most research has found no relationship, or an inverse relationship, between erosion rate and hardness, especially within metallic systems.[4,11–13] Research on the microstructural modification of steel has shown that an increase in hardness can increase the erosion rate[11,14] or have little to no effect. McCabe *et al.*[15] found that, for different microstructures (spheroidite, pearlite, martensite, and tempered martensite), there was little difference in the steady-state erosion rates of 1080 and 10105 steel.

There have been several limited studies on the erosion behavior of spheroidized steels. It has been found that wastage decreases significantly from the as-quenched condition to the quenched-and-tempered state,[11,16,17] and that additional tempering continues to decrease wastage for 1045 and 4140 steels.[16,17] Work reported by Levy[18] on the erosion of spheroidized 1020 steel at 30 deg impact found that the erosion rate changed with increasing carbide size and spacing. As the carbide spacing was increased from 3.4 μm (0.5-μm size carbides) to 5.67 μm (1.0-μm size carbides), the erosion rate decreased. Further tempering to a carbide spacing of 10 μm (3.0-μm size carbides) caused a large increase in erosion rate. This indicates that an optimum carbide size for minimizing erosion rates exists. A comparison of iron, 1020, and 1080 steel spheroidized to approximately 1.5 to 2.0 μm found that the addition of 3 pct carbide to pure iron reduced the erosion rate, but that additional carbide (12 pct) caused an increase in the erosion rate.[19] Again, it appears that an optimum morphology exists for erosion resistance of spheroidized steels. Finally, it was found[15] that the erosion rate of 1078 steel spheroidized to four carbide sizes, ranging from 0.7 to 1.7 μm, did not measurably change, and that comparison of 1078 and 10105 steels, spheroidized to 1.7 and 1.9 μm, respectively, also did not show a change in erosion rate.

The role of a second phase in a ductile matrix, especially that of spheroidized carbides in steel, on the erosion resistance is unclear. Some indications that an optimum morphology exists have been found, yet other results indicate that there may not be a change in erosion rate. It has been argued that the erosion rate cannot be changed by alloy manipulation due to the high strain rates that occur during erosion.[20] One strengthening mechanism that is not dependent on strain rate is grain size,[21] which may prove important in any correlation between mechanical properties and erosion resistance and may allow some forms of metallurgical modification, although limited testing on the effect of grain size with respect to erosion rate was inconclusive.[22] The iron–spheroidized carbide system is an ideal candidate for determining the role of morphology on erosion, since it is relatively easy to control and change carbide size, spacing, and grain size.

B.A. LINDSLEY, Senior R&D Engineer, is with the Special Metals Corp., New Hartford, NY 13413. A.R. MARDER, Professor, is with the Department of Materials Science and Engineering, Lehigh University, Bethlehem, PA 18015.

Manuscript submitted February 3, 1997.

Table I. Alloy Compositions and Austenitizing Temperatures Used for the Iron-Carbon Alloy Series

Alloy Designation	C	P	S	Mn, Si, Cr	Mo, V, Cu, Sn	Al	Ni	Austenitizing Temperature (°C)
A1	0.003	<0.003	0.004	<0.01	<0.002	<0.005	0.01	—
A2	0.20	<0.003	0.003	<0.01	<0.002	<0.005	0.01	1050
A3	0.40	<0.003	0.003	<0.01	<0.002	<0.005	0.02	950
A4	0.60	<0.003	0.004	<0.01	<0.002	<0.005	0.02	850
A5	0.80	<0.003	0.005	<0.01	<0.002	<0.005	0.02	825
A6	1.00	<0.003	0.005	<0.01	<0.002	<0.005	0.02	850
A7	1.22	<0.002	0.003	<0.01	<0.002	<0.005	0.02	950
A8	1.39	<0.002	0.003	<0.01	<0.002	<0.005	0.02	1025

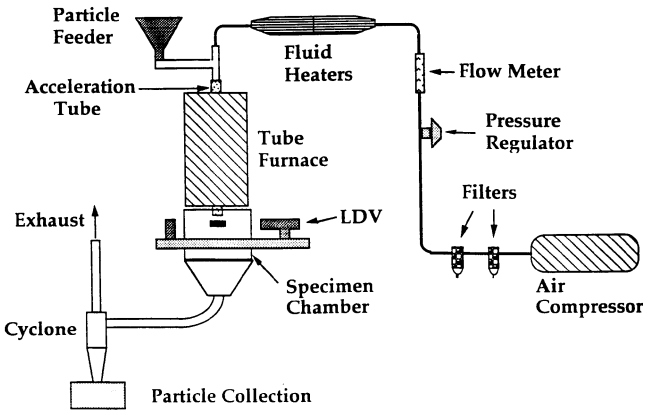

Fig. 1—Schematic diagram of the erosion test apparatus.

II. EXPERIMENTAL PROCEDURE

The materials used in this research were a series of iron-carbon alloys spanning the compositional range of 0.003 to 1.4 pct C in increments of 0.2 pct C (Table I). The materials were made by vacuum induction melting of electrolytic iron with graphite additions. The Fe-C alloys were placed in an environmental box furnace with a nitrogen environment and were austenitized at the temperatures found in Table I for 45 minutes. The samples were water quenched following the austenitization treatment to form martensite. One sample from each alloy group was sectioned, metallographically prepared, and etched in 2 pct nital to ensure that a martensitic structure formed. The pure Fe (0.003 pct C) samples, designated A1, were heated to 700 °C, held for 0.5 hours, furnace cooled to 600 °C, and then air cooled.

Tempering was performed at 690 °C using a tube furnace that was adapted for use with a controlled nitrogen environment. The nitrogen flow was kept at 100 mL/min for 0.5 hours, and then reduced to 10 mL/min for the duration of the temper. This treatment was found to minimize oxidation of the samples. The test sample was found to reach 600 °C in 5 minutes and the test temperature of 690 °C in 10 minutes. As rapid tempering occurs at temperatures above 600 °C, tempering time was considered to start after the samples had been in the furnace for 5 minutes. A decarburized layer in the alloys was found to occur in this test environment for temper times on the order of 1 week. To prevent decarburization, samples that were tempered for more than 8.64×10^4 s (24 hours) were vacuum encapsulated in a quartz tube prior to treatment. All samples were water quenched upon removal from the furnace, including the encapsulated samples that were broken underwater.

The tempered samples were sectioned, using an abrasive cut-off wheel, into two pieces, with one piece being cut and ground to 3/8 × 3/8 inches for erosion testing and the second metallographically prepared for light optical microscopy. The samples were ground and polished to 0.05 μm colloidal silica. For the carbide size measurements, the samples were etched in boiling alkali picric (25 g NaOH, 2 g picric, and 100 mL H_2O) for 2 minutes; for the ferrite boundary measurement, the samples were etched with Beraha's etchant (100 mL water, 10 g sodium thiosulfate, and 3 g potassium metabisulfide) for approximately 2 minutes.

A schematic diagram of the erosion test apparatus is given in Figure 1. The erodent is combined with the (hot) gas stream by way of a screw feeder and is accelerated to the test velocity down an SiC tube (15-mm i.d., 1.5-m length). Particle velocity is measured during the test using a laser doppler velocimeter. The impact angle can be varied over a range of angles ($0 \text{ deg} < \alpha \leq 90 \text{ deg}$), although 90 deg was used exclusively in this study. Additional information regarding the test apparatus can be found in Reference 23. The sample size was chosen to be 3/8 × 3/8 ± 0.005 inches and brown alumina was used as an erodent. The 46-grit brown alumina (96 pct Al_2O_3, 3 pct TiO_2), which has a size ranging from approximately 300 to 550 μm, was purchased and sieved to between 355 and 425 μm to minimize the size distribution. This narrower range was used for the erodent in this study. The erosion test conditions that were used in this study are a particle velocity of 40 m/s, a particle flux of 8.6 mg/mm^2/s, a temperature of 20 °C, and an impingement angle of 90 deg.

It was determined that a standard test specimen was needed in order to compare erosion rates from different test runs. Although the standard deviation in erosion rates was less than 0.5 pct for two identical samples tested on the same day, the erosion rate was found to change by as much as 10 pct over time, due to slight changes in the erosion test conditions. These changes were the result of the acceleration tube wearing away, thereby changing the particle flux. The 0.003C-Fe sample was, therefore, chosen as a standard and was tested each day with the rest of the specimens. The erosion rates were normalized to the pure iron standard utilizing the following equation:

$$ER_{\text{normalized}} = ER_{\text{measured}} \times (ER_{\text{standard}}/ER_{\text{Fe,measured}})$$

where $ER_{\text{normalized}}$ is the corrected erosion rate for the given alloy, ER_{measured} is the measured erosion rate for the alloy, ER_{standard} is the standard erosion rate for the pure iron, and $ER_{\text{Fe,measured}}$ is the erosion rate of the iron sample measured at the time the given alloy was tested.

In order to verify that these corrections were valid, supplemental tests were performed on the 0.6 and 1.4 pct C alloys. The three carbide sizes for each material were tested at the same time. It was found that, within the standard deviation, the percentage change in erosion rate between the three carbide sizes for each of the two alloys was the same for the corrected erosion rates and the supplemental tests. These tests verify that the corrections are valid and may be used to compare the erosion results between tests.

Erosion sample weight loss was measured using a balance sensitive to 0.1 mg. The samples were cleaned in acetone for 5 minutes after erosion testing using an ultrasonic cleaner and then weighed. The erosion process was repeated several times for each sample until a steady-state erosion rate could be accurately determined. Typical test intervals ranged from 30 to 45 minutes, with a total test time of approximately 4 hours for each sample.

Carbide size was determined using a quantitative image analysis system. The system digitizes an image from the microscope, and different gray levels are used to distinguish features. The etched carbides were thresholded by gray level and separated for analysis. Particle area (A) was measured and converted to an equivalent particle diameter (d) by the equation

$$d = \sqrt{(4/\pi * A)} \quad [1]$$

Ten fields of each sample were taken at a magnification of 1000 times for temper times up to 8.64×10^4 seconds, and at a magnification of 600 times for longer periods of time. The total number of particles measured ranged from approximately 600 to 10,000, depending on tempering time and alloy content. The mean free path (λ) was calculated using the following equation:[24]

$$\lambda = (2d/3f) * (1 - f)$$

where d is the particle diameter and f is the carbide volume fraction. The number of intersections of both ferrite-ferrite boundaries and ferrite-carbide boundaries per unit length of line (N_l) was determined using the Abram's three-circle method (ASTM E112). The value of N_l was then used to calculate the microstructural spacing (Λ), which is given by[25]

$$\Lambda = (1 - f)/N_l \quad [2]$$

All light optical micrographs in this study were taken using a Zeiss Axiomat metallograph. Secondary electron images of the eroded surface and cross-sectioned samples were taken using a JEOL* 6300 scanning electron microscope operated at 5 and 10 kV.

*JEOL is a trademark of Japan Electron Optics Ltd., Tokyo.

Microhardness measurements were made using a LECO* M-400FT microhardness tester. Measurements of the change in hardness with depth from the eroded surface were performed with a 10-g load, a Knoop indenter oriented parallel with the eroded surface, and indents every 10 μm. These conditions allowed for the closest hardness measurements to be made near the eroded surface and the development of a microhardness profile curve. Measurements of the overall base hardness were performed with a 500-g load, which sampled a large area, including both ferrite and carbide, and limited the error in the measurement due to difference in hardness between these constituents.

*LECO is a trademark of LECO Corporation, St. Joseph, MI.

III. RESULTS AND DISCUSSION

A. *Erosion Sample Morphology*

The Fe-C alloys were heat treated to form nominal carbide diameters of 0.4, 0.8, and 1.6 μm for the 0.2 and 0.4 pct C alloys and 0.8, 1.6, and 2.4 μm for the 0.6 to 1.4 pct C alloys. An example of the three carbide sizes is shown in Figure 2 for the 0.8 pct C alloy. The actual carbide diameters can be found in Table II; utilizing the size data and the carbide volume fraction, the mean free path was calculated. It has been shown in the literature[25] that the controlling factor on the mechanical properties of a spheroidized steel changes from carbide spacing to grain boundary control at low-carbide fractions. Since the mechanical properties of the material will likely affect the erosion resistance, the number of boundaries (both ferrite-ferrite boundaries and ferrite-carbide boundaries) per unit length was measured in the alloys, and the microstructural spacing was determined.

B. *Microstructural Effects on Erosion*

A total of 21 carbide-containing samples, plus the pure iron sample, were erosion tested. An example of the weight loss *vs* time plots, showing the 0.8 μm samples, is given in Figure 3. It can be seen in this graph that, of the carbide-containing materials, the 1.4 pct C sample has the lowest erosion rate, and the erosion rate increases as carbide content decreases, with the 0.2 pct C sample having the highest erosion rate. Samples containing 0.2 through 1.4 pct C show an incubation region, as the linear fits do not go though the origin. Although data were not acquired at times less than 30 minutes, an incubation time of approximately 20 minutes can be estimated. The pure iron sample shows little to no incubation on this figure. This sample had been used in previous experiments (under similar test conditions), and, therefore, one would not expect to see an incubation period, since the initial deformation required before erosion occurs already exists in this sample. The erosion rates for the 21 materials are given in Table III.

C. *Erosion Sample Cross Section*

The erosion samples were cross-sectioned to examine the surface and subsurface features incurred during the erosion process. Figure 4 shows the erosion surface of the pure Fe and the 1.4 pct C alloy in the 2.4 and 0.8 μm condition. A highly deformed peak-and-valley morphology was found at the surface. Extruded lips were seen in the peak regions, while the crater regions contained fragmented erodent particles and folded substrate material. It is theorized that the extruded lips are folded down onto the surface by subsequent impacts and entrap erodent fragments. In Figure 4(b), an elongated carbide running perpendicular to the surface, which has cracked during the test, can be seen. The carbide has cracked in several locations, and the end fragment (marked by the arrow) has been displaced due to the de-

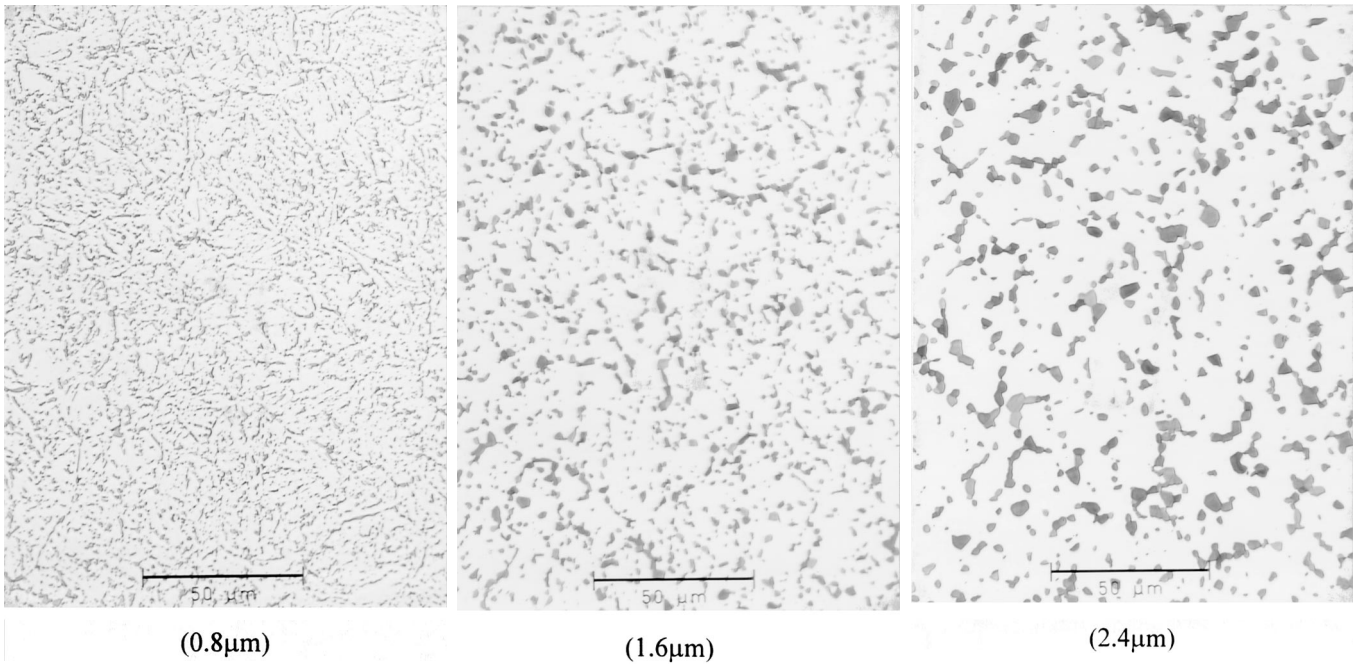

Fig. 2—The microstructures of the erosion samples revealing the carbide size and distribution for the 0.8 pct C alloy.

formation and material flow of the ferrite in the near-surface region, caused by the impacting particles. The 1.4 pct C material in the 0.8 μm condition (Figure 4(c)) was also examined and compared to the previous material in the 2.4 μm condition. The peak-and-crater feature is still evident, while the carbide cracking is less prevalent with the smaller carbides. No change in the erosion mechanism can be seen from these cross sections, which represent the boundary conditions of no carbide and the greatest amount of carbide in the smallest and largest particle sizes, respectively.

D. *Microhardness Profile*

Microhardness tests were performed on the cross-sectioned erosion samples. Hardness profiles from the eroded surface into the bulk material were made using a Knoop indenter with a 10-g load at 10 μm intervals. For the pure iron sample, an increase of hardness was found in the surface region, changing from 95 HKN in the bulk to 200 HKN near the surface, with a plastic zone depth of 100 μm (Figure 5). This is indicative of deformation and work hardening in the material. However, when the carbide-containing materials were tested, the harder carbides interfered with the hardness measurement of the matrix. Significant scatter can be seen for the 0.2 pct C material in the 0.8 μm condition, which has relatively few carbides. A lower bound has been drawn to estimate the hardness of the ferrite matrix, and a work-hardened zone is evident near the surface. The amount of scatter in the hardness data increased as the carbon content and number of carbides increased in the other alloys tested. No correlations between erosion rate and microhardness profile could be made for this reason, but it was noted that all samples showed some work hardening in the surface region.

The previous observations on the cross-sectioned samples and the microhardness profiles imply that erosion at a 90-deg impact is controlled, at least partially, by factors that affect ferrite deformation. If it is assumed that erosion is dependent on plastic deformation, then the microstructural features that affect dislocation motion should be examined. These features include grain boundaries and second-phase carbides, which are barriers to dislocation motion. If a relationship can be found linking erosion rate to a microstructural feature, then a direct structure-property relationship can be determined for erosion. Any relationships that could be drawn between the erosion rate and the mechanical properties of the material would exist due to their mutual dependence on the material microstructure (and, possibly, crystal structure, if different materials were tested).

E. *Carbide Spacing*

The normalized erosion rates at 90 deg for all materials are plotted *vs* carbide volume percent in Figure 6. The maximum error in the erosion rate measurement is 1.5 pct, which is smaller than the datum point, and, therefore, no error bars have been plotted. It can be seen that there is a dependence of both particle size and volume fraction on the erosion rate. A decreasing particle size leads to a decrease in erosion rate for all volume fractions. An increasing volume fraction of the second phase also leads to a decrease in erosion rate for volume percents greater than 6 pct. Below this amount, the effect of volume percent on erosion rate is governed by the particle size. At small particle sizes, erosion decreases as carbide volume percent is increased, but at large carbide sizes, the erosion rate increases as percent carbides is increased. These results suggest that erosion rate is dependent on a combination of carbide size and carbon content.

Figure 7 shows a plot of mean free path *vs* erosion rate. A relationship between erosion rate and λ was found, where decreases in λ caused decreases in the erosion rate. The data points for the 0.2 pct C alloy, given by the square data points, do not fit this relationship. Liu and Gurland[25] have

Table II. Average Carbide Size, Carbide Mean Free Path, and Microstructural Spacing for Each of the Erosion Samples

Percent Carbon	Nominal Carbide Size (μm)	Average Carbide Size (μm)	Mean Free Path λ (μm)	Microstructural Spacing, Λ (μm)
0.2	0.4	0.374	8.956	3.6484
0.4	0.4	0.435	4.791	2.7533
0.2	0.8	0.778	18.63	4.4170
0.4	0.8	0.725	7.985	3.6679
0.6	0.8	0.700	4.887	3.1674
0.8	0.8	0.885	4.442	2.7364
1.0	0.8	0.815	3.144	2.3105
1.2	0.8	0.856	2.648	1.9413
1.4	0.8	0.755	1.923	1.7752
0.2	1.6	1.672	40.04	4.8061
0.4	1.6	1.790	19.72	4.5353
0.6	1.6	1.855	12.95	4.9474
0.8	1.6	1.555	7.805	3.4778
1.0	1.6	1.554	5.996	2.7795
1.2	1.6	1.582	4.893	2.7146
1.4	1.6	1.432	3.648	2.3141
0.6	2.4	1.971	13.76	5.8054
0.8	2.4	2.452	12.31	5.4198
1.0	2.4	2.214	8.542	4.2289
1.2	2.4	2.529	7.823	4.1377
1.4	2.4	2.410	6.139	3.4712

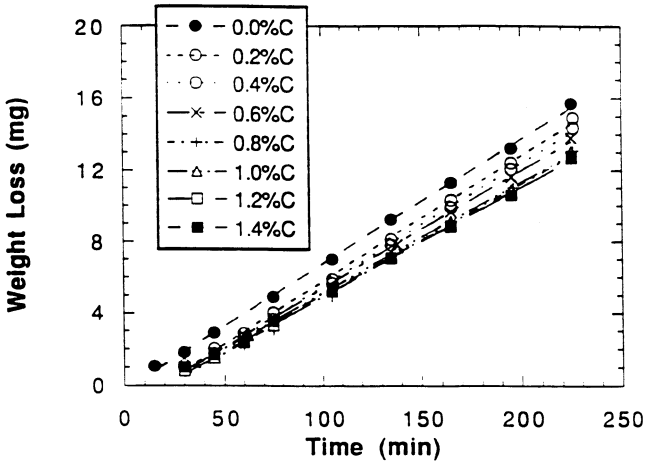

Fig. 3—Erosion weight loss *vs* time plot for pure iron and alloys 0.2 to 1.4 pct C in the 0.8 μm carbide condition at 90 deg impact. Erosion conditions: velocity, 40 m/s; temperature, 25 °C; erodent, 355 μm Al_2O_3; and feed rate, 90 g/min.

shown that the mechanical properties of spheroidized steels are governed by carbide spacing at carbon contents greater than 0.3 pct C and by grain size for carbon contents less than or equal to 0.3 pct C, so the departure of the 0.2 pct C alloy from the relationship between erosion rate and mean free path is not unexpected. This relationship shows that erosion rate is not directly dependent on absolute volume percent or carbide size, but that it is dependent on carbide spacing at carbon contents greater than or equal to 0.4 pct C.

The mechanical properties of spheroidized steels are dependent on the ferrite mean free path.[25–30] More specifically, the flow stress and hardness have been found to be dependent on a modified Hall–Petch relationship:

$$\sigma = \sigma_0 + k(d^*)^{-1/2} \quad [3]$$

where d^* is the grain size at low carbon contents (<0.3 pct); at higher carbon contents, d^* is related to the carbide spacing.[25,30] Microhardness measurements were made on the test samples to determine if these materials obeyed the same relationship. The bulk hardness measurements were made with a 500-g load and a Knoop indenter in the center of the samples. The 500-g load allowed for a hardness measurement that encompassed a large number of carbides. The hardness data was then plotted *vs* $\lambda^{-1/2}$ (Figure 8), and a linear relationship was found, given by the equation

$$H = 100.2 + 234.6\ \lambda^{-1/2} \quad [4]$$

where H is the microhardness and R^2, the correlation coefficient, is equal to 0.96. Again, the 0.2 pct C samples deviated from the best-fit line and were excluded from the previous equation, although the R^2 coefficient only dropped to 0.90 with the inclusion of this data. Using the hardness as a measure of flow stress and the overall mechanical properties of the material, it can be said that these materials follow the same relationship with carbide spacing as has been found by previous researchers.

As it has been assumed that erosion rate is dependent on carbide spacing in much the same way as other mechanical properties, it follows that a linear relationship would exist between erosion rate and $\lambda^{-1/2}$. The erosion rate was, therefore, plotted *vs* $\lambda^{-1/2}$, and the majority of the data were found to lie on a single line (Figure 9). Again, the 0.2 pct C samples were not within the linear fit. Another point that deviated from this relationship was the 1.4 pct C, 0.8 μm sample, which has the largest $\lambda^{-1/2}$ value. As mentioned in a companion paper on the characterization of these spheroidized structures (31), this sample consisted of both carbide films surrounding carbide-free ferrite plates and discreet carbide particles. This morphology led to errors in the mean free path measurement, and may explain the departure of the datum point from the linear relationship between $\lambda^{-1/2}$ and the erosion rate. When the 0.2 pct C and the 1.4 pct C, 0.8 μm data are excluded, a linear fit was found, given by the equation

Table III. Erosion Rates in Milligram/Minute for Each Alloy at Different Carbide Sizes (Erosion Rate for the Fe-0.003 Pct C Alloy Was 0.0698 mg/min)

Carbon Content	0.4 μm Carbides	0.8 μm Carbides	1.6 μm Carbides	2.4 μm Carbides
0.2	0.0680	0.0704	0.0710	—
0.4	0.0647	0.0690	0.0728	—
0.6	—	0.0657	0.0718	0.0724
0.8	—	0.0632	0.0693	0.0720
1.0	—	0.0619	0.0680	0.0703
1.2	—	0.0612	0.0653	0.0698
1.4	—	0.0603	0.0632	0.0687

$$\text{Erosion rate} = 0.082 - 0.035\ \lambda^{-1/2} \qquad [5]$$

where the error is given by an R^2 value of 0.96, which corresponds to a standard deviation of 7.2 pct. This result indicates that the erosion rate is dependent on the mean free path for carbon contents greater than or equal to 0.4 pct C, demonstrating that erosion resistance is directly related to the structure of the material. However, the issue of the 0.2 pct C alloys has not yet been addressed. Since it has been shown[25] that grain size controls the mechanical properties for carbon contents less than 0.3 pct C, and realizing that grain boundaries are also important with respect to dislocation motion, the effect of grain size on erosion was also examined.

F. *Microstructural Spacing*

Carbides are not the only barriers to dislocation motion in the material, as grain boundaries also play an important role. This is especially true considering that almost all of the carbide precipitates are located in the grain boundaries. It has been stated[25,30] that the grain and subgrain size is controlled by the particle spacing, due to particle pinning of the grain boundaries. However, a direct correlation has not been produced. The grain size can be measured in terms of the microstructural spacing ($\Lambda = (1 - f)/N_l$), which measures the distance between ferrite boundaries, including both ferrite grain boundaries and ferrite-carbide boundaries. This spacing is equal to the grain size for single-phase materials. Therefore, the mean free path was plotted *vs* the microstructural spacing to determine the effect of carbide spacing on grain size (Figure 10). The result of this plot is that, within error, a linear relationship exists between carbide spacing and grain size. The materials with large carbide spacings (the 0.2 pct C alloy in the 0.8 and 1.6 μm condition and the 0.4 pct C alloy in the 1.6 μm condition) deviate from this relationship. Clearly, the grain size of these materials is not controlled by the particle spacing. This results from the combination of a lack of carbide in the material, which can effectively pin the boundaries, and the large number of boundaries that formed from the lath martensite. This figure appears similar to Figure 7, in which erosion rate was plotted *vs* mean free path. The similar behaviors of grain size and erosion rate suggest that a relationship exists between the two.

The erosion rate was plotted *vs* microstructural spacing ($\Lambda^{-1/2}$) to determine the effect of grain boundaries on erosion (Figure 11). It was found that erosion rate decreased linearly as $\Lambda^{-1/2}$ increased, in much the same manner as mean free path. However, the distinctive feature of the 0.2 pct C alloys deviating from the rest of the data is no longer evident in Figure 11. By choosing Λ as the independent variable, all of the data can now be described. Similarly to the Hall–Petch relation for flow stress and microstructural spacing, the equation describing the relationship between erosion rate and Λ is given by

$$\text{Erosion rate} = 0.090 - 0.040\Lambda^{-1/2} \qquad [6]$$

The correlation coefficient for this equation, R^2, is equal to 0.92. It should be noted that this equation is only valid for this particular system and set of test conditions. Even so, this clearly demonstrates the erosion rate dependence on grain size.

This result may be somewhat surprising, in that erosion is generally thought of as a surface phenomenon, with material being removed incrementally from the eroded surface. The morphology of the highly deformed surface layer bears little resemblance to the bulk material, yet the bulk microstructure influences the erosion rate of Fe-C alloys by controlling the subsurface deformation response of the material. Work hardening was found well below the surface layer (10 to 15 μm deep) to a depth of 50 μm for the 0.2 pct C, 0.8 μm sample. It is in this region of 10 to 50 μm deep that the morphology plays an important role by presenting barriers to dislocation motion and affecting the plastic deformation response of the material. This, in turn, changes the number of impacts required for a given surface hardness or fracture stain to be reached, thereby affecting the erosion rate.

The erosion data for the pure iron sample do not fit on this microstructural spacing/erosion-rate curve and have not been included in the previous plots. It was found that the grain size of this material was 220 μm, which is approximately two orders of magnitude greater than the grain sizes for the 0.2 to 1.4 pct C alloys in this study. It is not clear what the effect of such a large grain size is, although it may involve the manner in which the dislocations can move through the material. If the dislocations that are generated in the surface region can move without encountering barriers such as carbides and grain boundaries, a large plastic zone size would be expected, as was found for the pure iron sample (Figure 5). Therefore, there may exist a grain size at which increases in grain size are no longer significantly detrimental to properties such as flow stress and may aid in allowing the dislocations to travel more deeply into the substrate. This effect would increase the energy absorbed in the material, thereby lowering the erosion rate. Results from Reddy and Sundararajan[22] have shown that, although grain size is not a significant factor in the erosion resistance of iron, with a grain size from 40 to 1100 μm, as compared to the erosion rate between different metals, there is a slight decrease in the erosion rate from 75 to 40

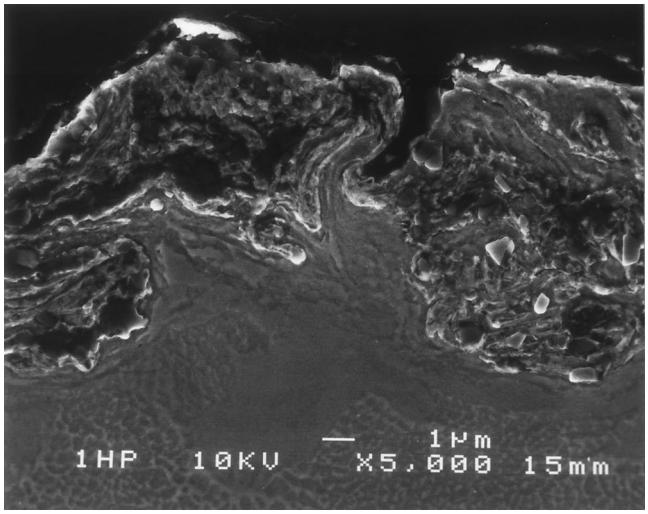

(*a*)

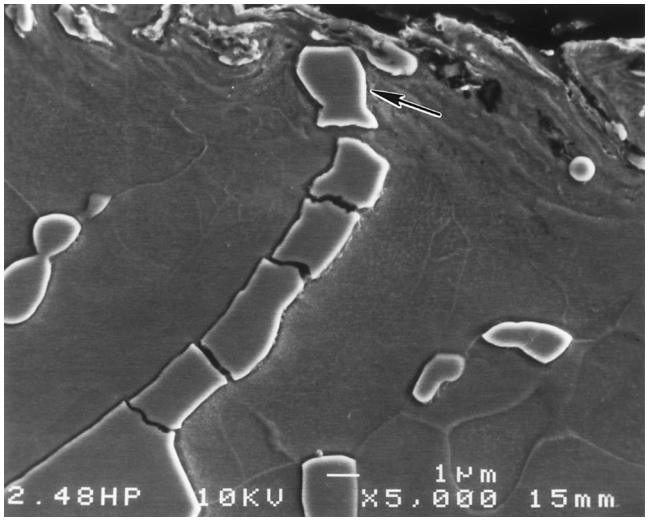

(*b*)

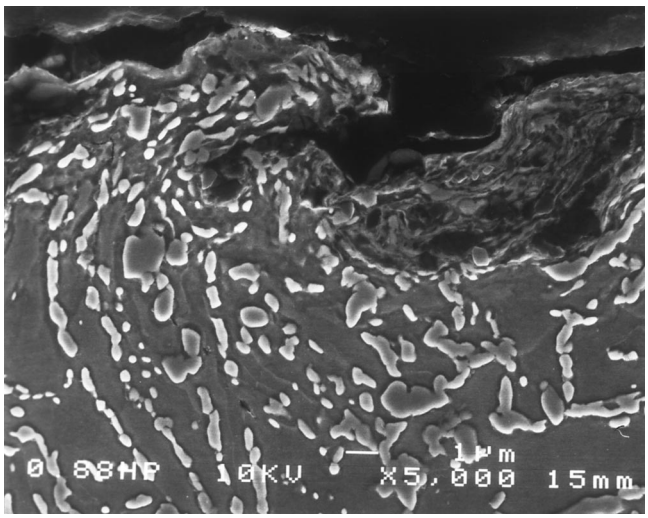

(*c*)

Fig. 4—Scanning electron and micrographs of cross-sectioned (*a*) pure iron and the 1.4 pct C alloy in the (*b*) 2.4 μm and (*c*) 0.8 μm carbide size eroded at 90 deg impact. Magnification 2000 times.

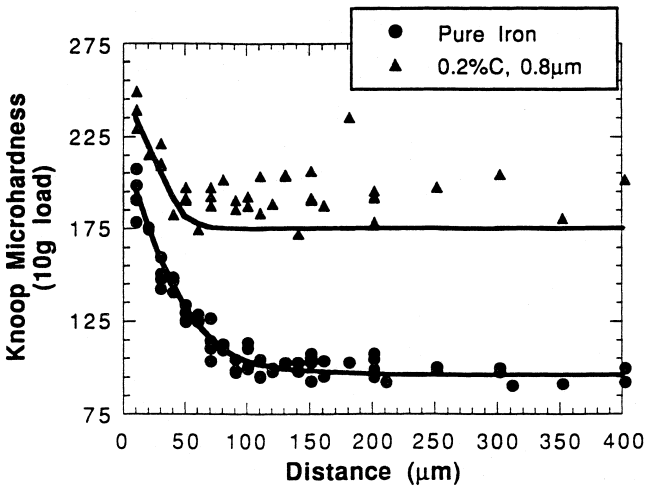

Fig. 5—Microhardness *vs* distance from the eroded surface for pure iron and the 0.2 pct C alloy in the 0.8 μm condition. Erosion conditions: velocity, 40 m/s; impact angle, 90 deg; temperature, 25 °C; erodent, 355 μm Al_2O_3; and feed rate, 90 g/min.

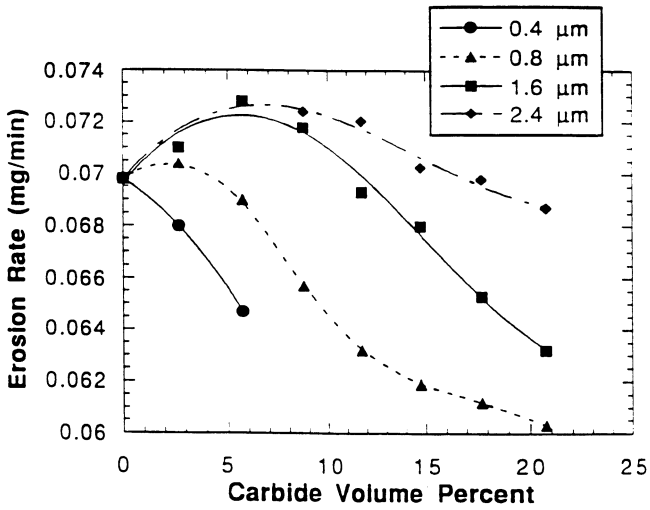

Fig. 6—Erosion rate *vs* carbide volume percent for pure iron and 0.2 to 1.4 pct C with their respective, nominal carbide sizes. Erosion conditions: velocity, 40 m/s; impact angle, 90 deg; temperature, 25 °C; erodent, 355 μm Al_2O_3; and feed rate: 90 g/min.

μm and from 75 to 550 μm. This indicates that there may be a grain size where the erosion rate is at a maximum and that sizes greater than and smaller than that size may have lower erosion rates. If so, this would explain the relatively low erosion rate found for the pure iron sample and justify the absence of the pure iron sample from the microstructural spacing/erosion-rate curve. The 0.2 to 1.4 pct C alloys have microstructural spacings below this maximum and follow a Hall–Petch relationship, while the pure iron sample has a spacing greater than this maximum and does not erode in a similar manner to the other alloys.

G. *Morphology Summary*

It has been shown that erosion is controlled by a deformation process at a normal impingement angle. The factors that affect this deformation process will, therefore, determine the erosion resistance. At first glance, it appeared as though carbide spacing was the microstructural variable

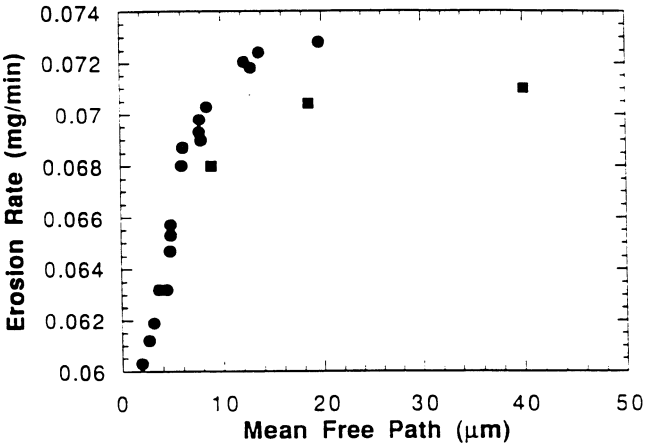

Fig. 7—Erosion rate *vs* mean free path. Alloy A2 (0.2 pct C) is given by the square data points. Erosion conditions: velocity, 40 m/s; impact angle, 90 deg; temperature, 25 °C; erodent, 355 μm Al_2O_3; and feed rate, 90 g/min.

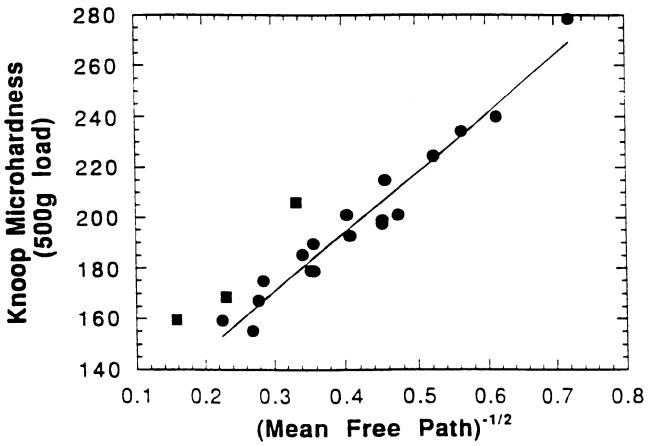

Fig. 8—Microhardness *vs* (mean free path)$^{-1/2}$ plot for alloys 0.2 to 1.4 pct C. Alloy A2 (0.2 pct C) is given by the square data points. Indents were made with a Knoop indenter and a 500-g load.

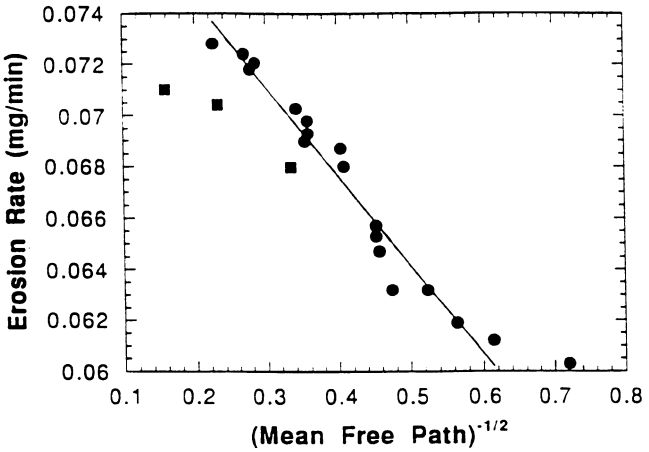

Fig. 9—Erosion rate *vs* (mean free path)$^{-1/2}$ plot for alloys 0.2 to 1.4 pct C. Alloy A2 (0.2 pct C) is given by the square data points. Erosion conditions: velocity, 40 m/s; impact angle, 90 deg; temperature: 25 °C; erodent, 355 μm Al_2O_3; and feed rate: 90 g/min.

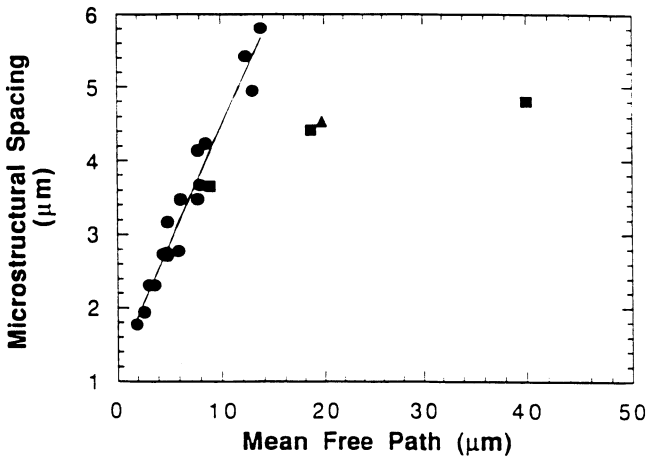

Fig. 10—A plot of microstructural spacing *vs* mean free path. Alloy 0.2 pct C is given by the square data points, and alloy 0.4 pct C, 1.6 μm is given by the triangle.

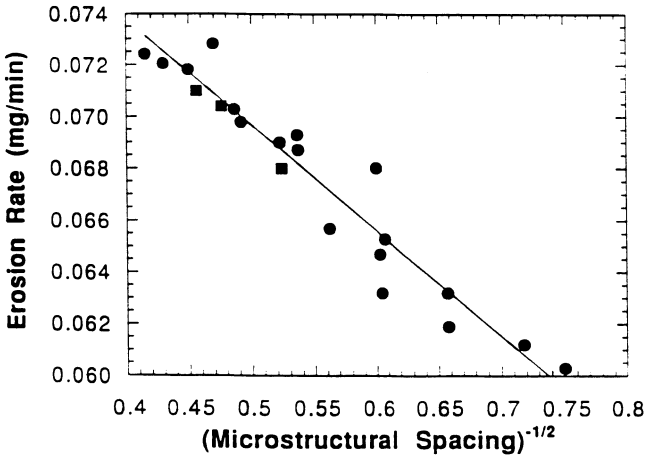

Fig. 11—Erosion rate *vs* (microstructural spacing)$^{-1/2}$ for alloys 0.2 to 1.4 pct C. Alloy 0.2 pct C is given by the square data points. Erosion conditions: velocity, 40 m/s; impact angle, 90 deg; temperature, 25 °C; erodent, 355 μm Al_2O_3; and feed rate, 90 g/min.

that controlled erosion. After further analysis, it was determined that microstructural spacing is the critical variable for erosion, as all of the data can be described by this variable.

The major effect of the carbide in these materials was to control the grain size. The absence of carbides within the grains results in little additional boundary that would act as a barrier for dislocation motion. Since the carbides reside in the grain boundaries, they can be considered as part of the boundary, which results in grain size being a critical variable for erosion. By increasing the amount of carbide and decreasing the particle size, the grain size was decreased and, therefore, so was the erosion rate. Hence, additional increases in the carbon content of spheroidized Fe-C alloys beyond the scope of this study may be beneficial for erosion resistance. This finding can be applied directly to metal-matrix composites, where particle size and content can be more easily controlled to produce a finer microstructure. However, a level of carbide will be reached at which the mechanical properties of the carbide become important. If a large enough portion of the boundary is in-

habited by carbides, then cracking of these carbides may result in ferrite grain removal with little energy absorption through plastic deformation of the ferrite. For the carbide contents and sizes used in this study, the cracking of the carbides appeared to have little effect on the erosion rate, but may be responsible for some of the scatter in the microstructural spacing/erosion-rate relationship.

IV. CONCLUSIONS

The following conclusions can be drawn from the results of this research on the erosion resistance of spheroidized Fe-C alloys.

1. It was determined that the distance between carbides controlled the erosion resistance of the material for carbon contents between 0.4 and 1.4 pct. A Hall–Petch relationship between mean free path and erosion rate was found. The hardness of the material was also found to follow a similar equation.
2. The ferrite grain and subgrain size were controlled by the carbide spacing for the 0.4 to 1.4 pct C alloys, except for the 0.4 pct C in the 1.6 μm carbide condition. The 0.2 and 0.4 pct C, 1.6 μm alloys were not found to depend on carbide spacing, as the spacing became too large relative to the small grain size that remained throughout tempering.
3. The erosion resistance of all carbide-containing alloys was found to depend on the microstructural spacing, which incorporated both the carbide spacing and the ferrite grain boundaries. This relationship can be described though a Hall–Petch-type equation.

$$\text{Erosion rate} = 0.090 - 0.040\Lambda^{-1/2} \qquad [7]$$

4. Erosion of spheroidized Fe-C alloys occurs by a plastic deformation mechanism. A peak-and-valley–type structure develops at the erosion surface, in which substrate is extruded up into the peaks, resulting in the formation of a lip. Subsequent particles impact the lip and cause it to become folded back down onto the surface. Erodent fragments become entrapped during this folding process, and the valleys fill with highly deformed ferrite, carbide, and erodent. Material is removed when the critical stress-strain conditions are met. Since the erosion is controlled by plastic deformation of the matrix, barriers that impede the movement of dislocations in the material, such as grain boundaries and carbides within the grains, *i.e.*, not those at the grain boundaries, determine the erosion resistance of these materials.

ACKNOWLEDGMENTS

The authors thank Mr. Arlan Benscoter for his assistance in the metallography lab. The authors would also like to thank Dr. Brian Smith and Kevin Stein for their assistance in the construction of the erosion apparatus.

REFERENCES

1. *Annual Book of ASTM Standards*, Standard Designation G40-92, ASTM, Philadelphia, PA, 1992, vol. 3.02, p. 160.
2. I.M. Hutchings: in *Erosion: Prevention and Useful Application*, ASTM Special Technical Publication 664, W.F. Adler, ed., ASTM, Philadelphia, PA, 1979, p. 49.
3. G.P. Tilly: *Wear*, 1972, vol. 19, p. 18.
4. A.V. Levy: *Wear*, 1986, vol. 108, p. 1.
5. A. Ball: *Wear*, 1983, vol. 91, p. 201.
6. G. Sundararajan: *Wear of Materials*, ASME, Fairfield, NJ, 1991, p. 111.
7. M. Rao, J. Keiser, and D. Wilson: *Scripta Metall.*, 1989, vol. 23, p. 1475.
8. B.F. Levin, J.N. DuPont, and A.R. Marder: in *Elevated Temperature Coatings: Science and Technology II*, N.B. Dahotre and J.M. Hanpikian, eds., TMS, Warrendale, PA, 1996.
9. I. Finnie, J. Wolak, and Y. Kabil: *J. Mater.*, 1967, vol. 2, p. 682.
10. Y. Oka and I.M. Hutchings: *Corr. Eng.*, 1990, vol. 39, p. 677.
11. G. Green, R. Taggart, and D.H. Polonis: *Metallography*, 1981, vol. 14, p. 191.
12. Y. Shida and H. Fujikawa: *Wear*, 1985, vol. 103, p. 281.
13. M. Naim and S. Bahadur: *Wear*, 1986, vol. 112, p. 217.
14. L.L. Brass: Master's Thesis, University of California, Berkeley, CA, 1977.
15. L.P. McCabe, G.A. Sargent, and H. Conrad: *Wear*, 1985, vol. 105, p. 257.
16. M.E. Gulden: *Proc. 5th Int. Conf. in Erosion by Liquid and Solid Impact*, Cambridge University Publishing, Cambridge, United Kingdom, 1983, pp. 31-1.
17. L. Ambrosini and S. Bahadur: *Wear*, 1987, vol. 117, p. 37.
18. A.V. Levy: *Wear*, 1981, vol. 68, p. 269.
19. A.J. Ninham and A.V. Levy: *Wear Conference*, Elsevier Sequoia Publishing, Lausanne, Switzerland, 1987, vol. 2, p. 825.
20. A. Ninham: *Wear*, 1988, vol. 121, p. 307.
21. J.D. Campbell: *Mater. Sci. Eng.*, 1973, vol. 12, p. 3.
22. A.V. Reddy and G. Sundararunjan: *Metall. Trans. A*, 1987, vol. 18A, pp. 1043-52.
23. B. Lindsley, K. Stein, and A.R. Marder: *Meas. Sci. Technol.*, 1995, vol. 6, p. 1169.
24. B.I. Edelson and W.M. Baldwin, Jr: *Trans. ASM*, 1962, vol. 55, p. 230.
25. C.T. Liu and J. Gurland: *Trans. AIME*, 1968, vol. 242, p. 1535.
26. A.M. Turkalo and J.R. Low, Jr.: *Trans. AIME*, 1958, vol. 212, p. 750.
27. L. Anand and J. Gurland: *Metall. Trans. A*, 1976, vol. 7A, pp. 191-97.
28. R. Kossowsky and N. Brown: *Trans. AIME*, 1965, vol. 233, p. 1389.
29. Y.W. Chang and R.J. Asaro: *Met. Sci.*, 1978, June, p. 277.
30. P.C. Jindal and J. Gurland: *Metall. Trans.*, 1974, vol. 5, pp. 1649-53.
31. B.A. Lindsley and A.R. Marder: *Acta Mater*, 1998, vol. 46, p. 341.